THE JOURNAL OF BIOLOGICAL CHEMISTRY VOL. 282, NO. 13, pp. 9846–9854, March 30, 2007

Impact of Carrier Stiffness and Microtopology on Two-dimensional Kinetics of P-selectin and P-selectin Glycoprotein Ligand-1 (PSGL-1) Interactions*

Received for publication, September 28, 2006, and in revised form, December 29, 2006 Published, JBC Papers in Press, January 31, 2007, DOI 10.1074/jbc.M609219200

Li Wu[1,2], **Botao Xiao**[1,3], **Xiaoling Jia, Yan Zhang, Shouqin Lü, Juan Chen, and Mian Long**[4]

From the National Microgravity Laboratory and Center for Biomechanics and Bioengineering, Institute of Mechanics, Chinese Academy of Sciences, Beijing 100080, China

Mechanics and surface microtopology of the molecular carrier influence cell adhesion, but the mechanisms underlying these effects are not well understood. We used a micropipette adhesion frequency assay to quantify how the carrier stiffness and microtopology affected two-dimensional kinetics of interacting adhesion molecules on two apposing surfaces. Interactions of P-selectin with P-selectin glycoprotein ligand-1 (PSGL-1) were used to demonstrate such effects by presenting the molecules on three carrier systems: human red blood cells (RBCs), human promyelocytic leukemia HL-60 cells, and polystyrene beads. Stiffening the carrier alone or in cooperation with roughing the surface lowered the two-dimensional affinity of interacting molecules by reducing the forward rate but not the reverse rate, whereas softening the carrier and roughing the surface had opposing effects in affecting two-dimensional kinetics. In contrast, the soluble antibody bound with similar three-dimensional affinity to surface-anchored P-selectin or PSGL-1 constructs regardless of carrier stiffness and microtopology. These results demonstrate that the carrier stiffness and microtopology of a receptor influences its rate of encountering and binding a surface ligand but does not subsequently affect the stability of binding. This provides new insights into understanding the rolling and tethering mechanism of leukocytes onto endothelium in both physiological and pathological processes.

Selectins are important adhesive molecules that mediate the cell adhesions in such biological processes as platelet thrombosis, inflammatory responses, as well as tumor metastasis (1, 2). For example, selectin-ligand interactions mediate the rolling and tethering of leukocytes onto endothelium in blood flow. Three known selectin members, P-, E-, and L-selectin, have a common structure: an N-terminal, calcium-type lectin (Lec)[5] domain, followed by an epidermal growth factor (EGF)-like module, multiple copies of consensus repeat (CR) units characteristic of complement binding proteins, a transmembrane segment, and a short cytoplasmic domain (3, 4). As a biochemically well-characterized selectin ligand, P-selectin glycoprotein ligand-1 (PSGL-1) consists of homodimer cross-linked by disulfate bonds and binds to selectins through its N-terminal sulfoglycopeptide, which includes three tyrosine sulfates and the core-2 *O*-glycan (5–8).

To mediate cell adhesion, receptors and their ligands must be anchored onto two apposed surfaces, which is the so-called two-dimensional interaction. This is different from three-dimensional binding, where at least one of the receptors and ligands is in the fluid phase. Not only is two-dimensional kinetics of receptor-ligand binding determined by their intrinsic structures, but it also depends on their surface presentation as well as the stiffness and microtopology of molecule-bearing carrier. On the one hand, randomizing the selectin construct or rabbit immunoglobulin G (rIgG) or lowering the length of selectin extending outward from the cell surface significantly reduces the two-dimensional forward rate, but not reverse rate, of selectin-ligand or CD16-rIgG interactions (9). HL-60 cells adhere to immobilized full-length E-selectin, which contains all six CRs, but not to shorter E-selectin constructs with two or less CRs. However, they bind to the short E-selectin constructs with two or less CRs when they are captured by a nonblocking monoclonal antibody (mAb) adsorbed on the plastic surface (6). On the other hand, the stiffness and microtopology of the molecule-bearing carrier onto which receptors and ligands are anchored influence cell adhesion mediated by receptor-ligand binding. For example, CD16b molecules coupled onto relatively smoother human red blood cells (RBCs) bind to their human IgG ligand with a ~50-fold increase in two-dimensional effective affinity over those transfected onto relatively rougher Chinese hamster ovary (CHO) cells or human erythroleukemia K562 cells (10). Compared with intact neutrophils with the soft and rough configuration and fixed neutrophils with the relatively stiff and rough configuration, stiff and smooth PSGL-1-bearing microbeads roll faster and dissociate briefly over P-selectin-immobilized substrate (11). Cytochalasin B treatment or

* This work was supported by National Science Foundation of China Grants 30225027 and 10332060, and Chinese Academy of Sciences Grants 2005-1-16 and KJCX2-SW-L06. The costs of publication of this article were defrayed in part by the payment of page charges. This article must therefore be hereby marked "*advertisement*" in accordance with 18 U.S.C. Section 1734 solely to indicate this fact.

[1] Both authors contributed equally to this work.

[2] On leave from the College of Bioengineering, Chongqing University, Chongqing 400044, China.

[3] Current address: Dept. of Physics, University of Illinois at Chicago, Chicago, Illinois 60607.

[4] To whom correspondence should be addressed. Tel.: 86-10-6261-3540; Fax: 86-10-6261-3540; E-mail: mlong@ imech.ac.cn.

[5] The abbreviations used are: Lec, lectin domain; EGF, epidermal growth factor; CR, consensus repeat; PSGL-1, P-selectin glycoprotein ligand-1; RBC, red blood cell; $CrCl_3$, chromium chloride; FITC, fluorescein isothiocyanate; mIgG, hIgG, and rIgG, mouse, human, and rabbit immunoglobulin G; sPs, P-selectin construct consisting of Lec-EGF domains plus nine CRs; CHO, Chinese hamster ovary; mAb, monoclonal antibody.

hypotonic swelling of neutrophils disrupts the tethering to and enhances the rolling on E- or P-selectin-immobilized substrate in shear flow, probably because of a likely increase in the area of cell-substrate contact (12). Extensible microvilli, in contrast to rigid and non-extensible microvilli, reduced the pulling forces imposed on L-selectin-PSGL-1 bonds and facilitate the tether formation and rolling on endothelium (13). However, the effects of carrier stiffness and microtopology on two-dimensional binding have not been quantified systematically.

To test this possibility, three molecule-bearing carriers: RBCs with deformable membrane and relatively smooth surfaces, human promyelocytic leukemia HL-60 cells with less deformable membrane and rough surfaces, and polystyrene beads with stiff and smooth surfaces, were used in the current work. P-selectin and PSGL-1 were, respectively, coated or expressed onto the carrier surface with distinct stiffness and microtopology, and the effect on two-dimensional kinetics of P-selectin-PSGL-1 binding was investigated. Our results indicated that the carrier stiffness and microtopology influence the two-dimensional forward rate but not the reverse rate of the molecule of interest, whereas they have no effect on three-dimensional affinity. These results provide insights into the biophysical mechanisms by which the carrier stiffness and microtopology affect cell adhesion.

EXPERIMENTAL PROCEDURES

Cells, Beads, and Proteins—Human RBCs were isolated from whole blood of normal healthy volunteers as previously described (14). Briefly, ~5 ml of whole blood was collected by venipuncture into sterile tubes containing EDTA. This was centrifuged (30 min, 700 × *g*, room temperature), and the supernatant was removed. The pelleted RBCs were washed twice in RBC storage solution (EAS45+) (15) and stored aseptically at 4 °C in EAS45+ for up to 2 weeks with negligible hemolysis. Human promyelocytic leukemia HL-60 cells from ATCC were grown in RPMI 1640 medium supplemented with 2 mM L-glutamine, 100 units/ml penicillin, 10 μg/ml streptomycin, and 10% fetal bovine serum. HL-60 cells constitutively express PSGL-1 ligands for P- and E-selectin. Streptavidin-coupled polystyrene beads with a diameter of ~5 μm were purchased from Bangslabs Inc.

Soluble P-selectin (sPs) consisting of Lec-EGF domains plus nine CRs, but no transmembrane or cytoplasmic domains (16), anti-P-selectin blocking (G1) and capturing (S12) (17) mAbs, and anti-PSGL-1 blocking (PL1) and non-blocking (PL2) mAbs (5) (all mouse IgG1, mIgG1) were generous gifts from Dr. Rodger P. McEver (Oklahoma Medical Research Foundation). PSGL-1 constructs were purified following a modified protocol previously reported (18), and the purity of the proteins were analyzed by SDS-PAGE on 7.5% polyacrylamide gels followed by silver staining. Anti-CD58 mAb TS2/9 (mIgG1) was a generous gift from Dr. Periasamy Selvaraj (Emory University School of Medicine) (19). Fluorescein isothiocyanate (FITC)-labeled anti-P-selectin mAb G1 was purchased from Ancell Corp. (Bayport, MN). FITC-labeled goat anti-mouse antibody and the irrelevant control mIgG1 were from Sigma.

Coupling Proteins onto RBCs or Beads—A modified chromium chloride ($CrCl_3$) method described previously was used to couple mIgG1 or capturing mAbs (S12 or PL2) onto the surface of fresh human RBCs (9, 20). The coupling efficiency of proteins was examined by flow cytometry, using CD58, which is constitutively expressed on RBCs at a known density as a standard (21). The capturing mAb-coated RBCs were first incubated with 50–200 ng/ml of respective P-selectin and PSGL-1 constructs for 30 min at room temperature before being used in micropipette aspiration measurements, whereas mIgG1-coated RBCs were incubated with the same proteins and used as a control.

To form a biological force probe, the biotinylated capturing mAbs (S12 or PL2) were coupled onto the surface of a streptavidin-coated polystyrene bead, and the bead was then linked to a biotinylated human RBC (cf. Fig. 2, *d′* and *e′*). A biotinylation method described previously (22) was modified to biotinylate the capturing mAbs and RBCs. Briefly, NHS-LC-Biotin (Pierce) was dissolved into dimethyl formamide to a final concentration 5 ~ 10 mM. 3–5 μl of NHS-LC-Biotin solution in dimethyl formamide were added into 300 μl of capturing mAb solution in a concentration of 50 μg/ml or 190 μl of RBC suspension in a concentration of ~10^7/ml. After 30 min of incubation, the capturing mAb solution was eluted via a D-Salt Dextran Desalting Column (Pierce) in phosphate-buffered saline to exclude the unbound NHS-LC-Biotin, and the biotinylating efficiency was confirmed using an ImmunuPure® HABA kit (Pierce). Biotinylated RBCs were directly washed three times in phosphate-buffered saline and then stored in EAS45+ in ~10^7/ml. The biotinylated capturing mAbs and RBCs can be stored for several months and one or two weeks, respectively. Next, 5 μl of biotinylated capturing mAbs (S12 or PL2) at 30 μg/ml were mixed with 300 μl of streptavidin-coated beads in ~10^7/ml for 30 min at room temperature. After washing three times in phosphate-buffered saline, collected beads were segregated into two sets: one set of ~10^4 beads was resuspended and incubated with soluble sPs or PSGL-1 proteins at the final concentration of 350 ng/ml; after washing once in PBS, the collected beads were ready for micropipette aspiration measurements. Another set was used to determine the site densities of the molecules of interest (see below).

Site Density Determination—Site densities of surface proteins coated on RBCs or beads or expressed on HL-60 cells were determined using flow cytometry and/or immunoradiometric assay (IRMA) (23). To measure densities of G1- or PL1-coated via $CrCl_3$ coupling, RBCs were incubated directly with FITC-conjugated goat anti-mouse antibody (4.7 equivalent of FITC per IgG) at a concentration of 10 μg/ml in 200 μl of FACS buffer (RPMI, 5 mM EDTA, 1% bovine serum albumin, 0.02% sodium azide) on ice for 40 min. To measure the PSGL-1 expression, HL-60 cells were incubated first with anti-PSGL-1 mAb PL1 and then with FITC-conjugated goat anti-mouse secondary antibody (4.4 equivalent of FITC per IgG). After washing, the cells were analyzed by flow cytometry (Fig. 1*a*, *inset*). Site densities were then calculated by comparing the fluorescence intensities of the cells with those of standard beads (Bangslabs) (9, 24) (Fig. 1*a*). To measure densities of P-selectin or PSGL-1 coupled by capturing mAb-coated RBCs or beads, one set of RBCs or beads precoated with a range of densities of the relevant capturing mAb (three or four densities for each protein)

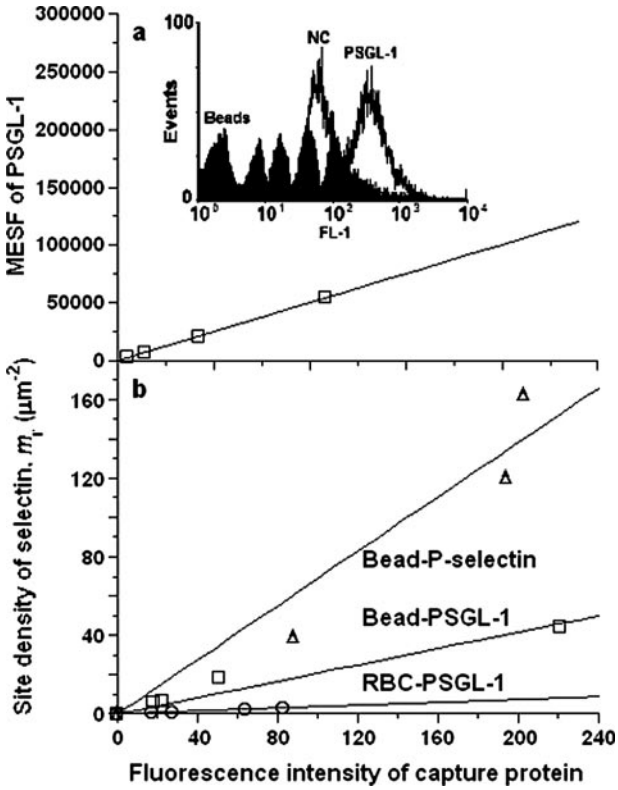

FIGURE 1. **Site density determination.** *a*, flow cytometry was used to determine site density of PSGL-1 constitutively expressed on HL-60 cells and G1- and PL1-coated RBCs. The calibration curve of standard beads was plotted as molecules of equivalent soluble fluorochromes (*MESF*) against fluorescence intensity of beads measured by cytometry (*inset*, filled histograms labeled *Beads*) using the manufacturer-provided program. Fluorescence intensity of PSGL-1 was measured from the cytometry (*inset*, unfilled histogram labeled *PSGL-1*), and the site density was estimated from calibration curves of standard beads after subtracting the negative control (*inset*, open histogram labeled *NC*). *b*, combined immunoradiometric and flow cytometry assays were employed to determine site densities of P-selectin or PSGL-1 captured by capturing mAbs (S12 or PL2) precoated on RBCs or beads. The calibration curve was plotted as site density of P-selectin or PSGL-1, determined using an immunoradiometric assay, against fluorescence intensity of the capturing mAbs (S12 or PL2), measured using the flow cytometry assay. Data for P-selectin on beads (*open triangles*) and PSGL-1 on beads (*open squares*) and RBCs (*open cycles*) were, respectively, fitted with straight lines (*solid lines*).

were incubated with FITC-conjugated goat anti-mouse antibody, and the fluorescence intensities were measured using flow cytometry as above. Another set of RBCs or beads precoated with the same range of densities of capturing mAb were incubated with the corresponding P-selectin or PSGL-1, and their site densities were measured by IRMA (9, 16). A calibration curve was obtained for each protein by plotting the protein site density against the mean fluorescence intensity of the capturing mAb (Fig. 1*b*), thereby allowing calculation of the site densities of protein of interest from the mean fluorescence intensities of the capturing mAb.

Micropipette Aspiration Assay—A micropipette adhesion frequency assay was used to measure the two-dimensional kinetics of P-selectin-PSGL-1 interactions (9, 14, 24, 25). Five systems were used to quantify the effect of carrier stiffness and microtopology: a P-selectin-coated RBC interacting with a PSGL-1-coated RBC (RBC-RBC) (Fig. 2, *a* and *a′*), a P-selectin-coated RBC interacting with a PSGL-1-expressing HL-60 cell (RBC-HL-60) (Fig. 2, *b* and *b′*) (9), a P-selectin-coated RBC interacting with a PSGL-1-coated bead (RBC-Bead) (Fig. 2, *c* and *c′*), a P-selectin-coated bead interacting with a PSGL-1-expressing HL-60 cell (Bead-HL-60) (Fig. 2, *d* and *d′*), and a P-selectin-coated bead interacting with a PSGL-1-coated bead (Bead-Bead) (Fig. 2, *e* and *e′*). Briefly, molecular carriers were distributed in a hypo-osmotic solution at an osmolarity of 175 mOsm (H_2O:HBSS = 1:1.4) to swell the RBC (some experiments were done at 200 and 150 mOsm). Two molecular carriers were, respectively, aspirated by two micropipettes at a suction pressure of 4 mm H_2O (some measurements were done at 8 and 12 mm H_2O) and were staged by placing them onto controlled contact via micromanipulation. The adhesion at the end of a given contact period was observed microscopically from the deflection of the flexible RBC membrane upon retracting it away from the RBC or HL-60 cell or the bead. Such a contact-retraction cycle was repeated a hundred times per pair to estimate the adhesion probability, P_a, at that contact duration, t. For each case examined, ~40 pairs of cells or beads were used to obtain several P_a *versus* t curves that correspond to different receptor and ligand densities, m_r and m_l. Each binding curve was fitted to a small system probabilistic kinetic model (9, 14, 24–27) shown in Equation 1,

$$P_a = 1 - \exp\{-m_r m_l A_c K_a^0[1 - \exp(-k_r^0 t)]\} \qquad \text{(Eq. 1)}$$

to estimate a pair of parameters: the zero-force reverse rate, k_r^0 and effective binding affinity, $m_l A_c K_a^0$ (if m_r was known) or $A_c K_a^0$ (if both m_r and m_l were known), where A_c is the contact area, which was kept constant in all experiments. Multiple pairs of (k_r^0, $m_l A_c K_a^0$) or (k_r^0, $A_c K_a^0$) values were obtained for each stiffness and microtopology to allow evaluation of the mean and standard deviation. The statistical significance (or the lack thereof) of the difference between the two-dimensional affinities (or reverse rates) of the P-selectin-PSGL-1 pair presented with different carrier stiffness and microtopology was assessed using the Student's *t* test.

In one set of experiments, adhesion frequencies between RBCs coated with G1 via $CrCl_3$ coupling and P-selectin-coated RBCs or beads or between RBCs coated with PL1 via $CrCl_3$ coupling and PSGL-1-expressing HL-60 cells or PSGL-1-coated beads were measured at a single contact time of 4 s, and the results were expressed as $y = -\ln(1 - P_a)/(m_r \times m_l)$. 5–6 pairs of cells were measured for each case, and the statistical significance of the differences between the results from different conditions were assessed by the Student's *t* test.

Scatchard Analysis—Scatchard analysis was used to determine three-dimensional binding affinities of ^{125}I-labeled G1 or PL1 mAb in the fluid phase for either sPs or PSGL-1 constructs coated on RBC or bead surfaces by precoated capturing mAbs (S12 or PL2) or expressed on HL-60 cells (9, 17, 28). Briefly, 200 μl of 0.1–6 μg/ml ^{125}I-G1 or ^{125}I-PL1 was added to ~5×10^6 cells or beads. After incubation at 4 °C for 30 min, 500 μl of a 2:8 ratio of GS-1 sealing oil (Sifang Oil Inc., Beijing): dibutyl phthalate (Sigma) oil mixture was added into each sample, which was then centrifuged to separate the free ^{125}I-G1 or ^{125}I-PL1 from the cells or beads. Radioactivity associated with the cell pellets or packed beads was measured using a γ-counter. Specific binding of G1 or PL1 mAb was calculated by subtracting the

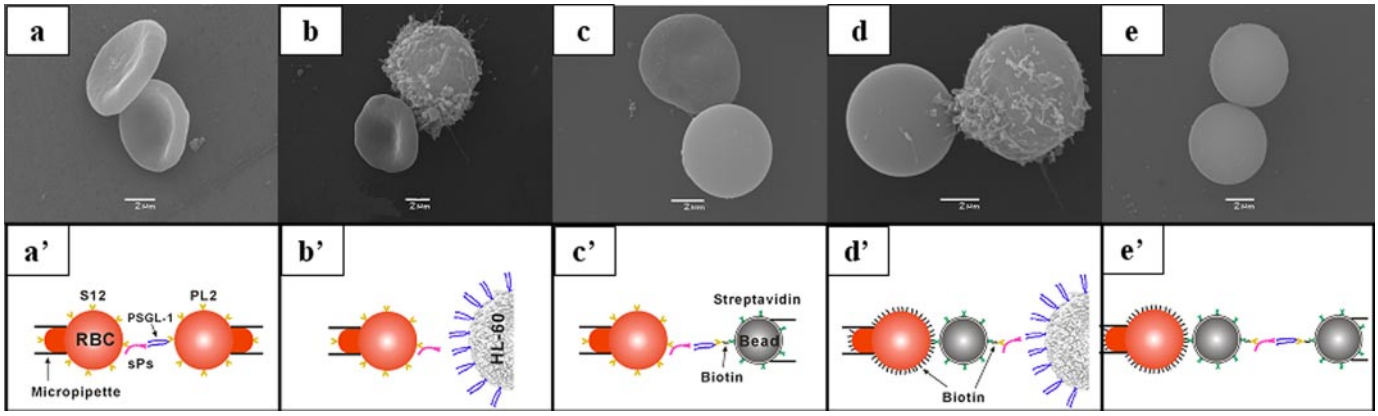

FIGURE 2. **Experimental configurations.** *a* and *a′*, binding of an RBC coated by sPs captured via S12 to another RBC coated by PSGL-1 captured via PL2. *b* and *b′*, binding of an RBC coated by sPs captured via S12 to an HL-60 cell expressing PSGL-1. *c* and *c′*, binding of an RBC coated by sPs captured via S12 to a bead coated by PSGL-1 captured via PL2. *d* and *d′*, binding of a bead coated by sPs captured via S12 and cross-linked to an RBC via biotin-streptavidin coupling to an HL-60 cell-expressing PSGL-1. *e* and *e′*, binding of a bead coated by sPs captured via S12 and cross-linked to an RBC via biotin-streptavidin coupling to a bead coated by PSGL-1 captured via PL2. *Upper panels* (*a*–*e*) are scanning electron microscopic images, and *lower panels* (*a′*–*e′*) are schematics of micropipette aspiration assay for each configuration.

nonspecific binding. All assays were performed in triplicate. The statistical significance of the difference between three-dimensional affinities of the G1-P-selectin and the PL1-PSGL-1 pair presented with different carrier stiffness and microtopology was assessed using the Student's *t* test.

RESULTS

Binding Is Specifically Mediated—The adhesion frequency at sufficiently long contact time ($t \rightarrow \infty$) was used to quantify the binding in control experiments. As exemplified for P-selectin-PSGL-1 binding in the RBC-RBC configuration (Figs. 2*a*, 2*a′*, and 3*a*), adhesion frequencies measured using the micropipette assay were mediated by specific P-selectin-PSGL-1 interactions, because they were present when the RBCs were coated with S12 and PL1 mAbs to capture P-selectin and PSGL-1 constructs, respectively, but were abolished when P-selectin or PSGL-1 constructs were absent. In addition, binding was blocked by mAbs against PSGL-1 (PL1), P-selectin (G1), and by the calcium chelator EDTA (Fig. 3*a*). Binding specificity for the other four configurations of RBC-HL-60 (Fig. 2, *b* and *b′* and Ref. 9), RBC-Bead (Figs. 2*c*, 2*c′*, and 3*b*), Bead-HL-60 (Figs. 2*d*, 2*d′*, and 3*c*), and Bead-Bead (Figs. 2*e*, 2*e′*, and 3*d*) were confirmed by similar experiments.

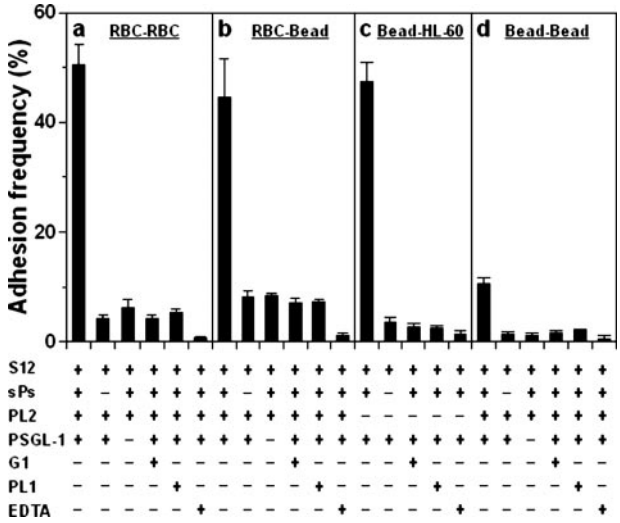

FIGURE 3. **Binding specificity.** A carrier (RBC or bead) coated by sPs captured via S12 bound specifically to another carrier (RBC or bead) coated by PSGL-1 captured via PL2 or an HL-60 cell expressing PSGL-1. The adhesion was abolished when PSGL-1 or sPs was absent or when anti-PSGL-1 mAb PL1 or anti-P-selectin mAb G1 or EDTA was present. Data are presented as the means ± S.E. of probability at $t \rightarrow \infty$. The symbols (+) and (−) represent the presence and absence of that protein or reagent, respectively.

Binding Follows Simple Kinetics—Contact duration dependence of adhesion frequency was measured using the micropipette assay at contact times ranging from 0.25–7 s in four configurations of RBC-RBC (Fig. 4*a*), RBC-Bead (Fig. 4*b*), Bead-HL-60 (Fig. 4*c*), and Bead-Bead (Fig. 4*d*). Site densities used were systematically varied by varying the amount of coated capturing mAb (S12 or PL2), as summarized in the *inset* in Fig. 4*d*. The adhesion probability, P_a, was obtained by removing the nonspecific adhesion frequency, P_n (*dashed lines* in Fig. 4, *a*–*d*, obtained by fitting the directly measured nonspecific adhesion frequency to Eq. 1), from the directly measured total adhesion frequency, P_t, according to $P_a = (P_t - P_n)/(1 - P_n)$. Similar to those described previously for RBC-HL-60 configuration (9), the data (*points* in Fig. 4, *a*–*d*) exhibited with a transient phase where P_a increased with *t* and a steady phase where P_a reached equilibrium. For each configuration of distinct stiffness and microtopology, Eq. 1 was used to best fit each binding curve to obtain two kinetic parameters of k_r^0 and $A_cK_a^0$. The mean reverse rate and effective binding affinity were calculated from two pairs of k_r^0 and $A_cK_a^0$ values at two densities of receptors. The mean k_r^0 and $A_cK_a^0$ values were then used, along with the corresponding m_r and m_l values measured from independent experiments, to predict each P_a *versus t* curve (*solid lines* in Fig. 4, *a*–*d*). It is evident that the model fits the data well.

Carrier Stiffness Affects Two-dimensional Forward Rates but Not Reverse Rates—To alter the stiffness of molecular carrier, PSGL-1 constructs were coated on a soft RBC and a stiff bead via capturing by precoated mAb PL2, respectively, and then bound to a P-selectin-coated RBC to form two configurations of RBC-RBC (Fig. 2, *a* and *a′*) and RBC-Bead (Fig. 2, *c* and *c′*). For each configuration, densities of P-selectin binding sites were quantified using adhesion-blocking mAbs, and P_a *versus t*

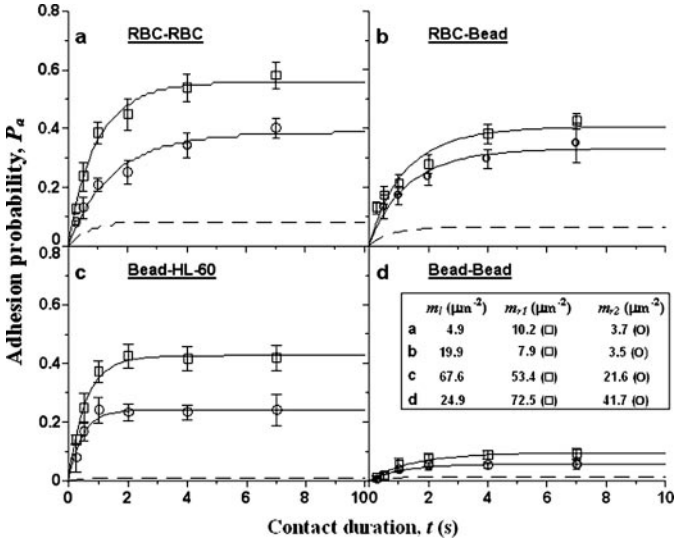

FIGURE 4. **Binding curves.** Adhesion probability was plotted against contact duration at different site densities, summarized in the *inset* in *panel d*, of $m_l \times m_r = 4.9 \times 10.2$ and 4.9×3.7 μm^{-4} for RBC-RBC (*a*), $m_l \times m_r = 19.9 \times 7.9$, and 19.9×3.5 μm^{-4} for RBC-Bead (*b*), $m_l \times m_r = 67.6 \times 53.4$, and 67.6×21.6 μm^{-4} for Bead-HL-60 cells (*c*), and $m_l \times m_r = 24.9 \times 72.5$ and 24.9×41.7 μm^{-4} for Bead-Bead (*d*) configuration. Experimental data (*points*), presented as the means ± S.E. at each contact time and obtained from 27–33 cell pairs for each curve, were compared with the predictions (*solid lines*) calculated from Equation 1 using the best-fit kinetic parameters and the corresponding $m_l \times m_r$ values. The *dashed line* represents nonspecific binding, obtained by fitting Equation 1 to nonspecific data (not shown for the sake of clarity).

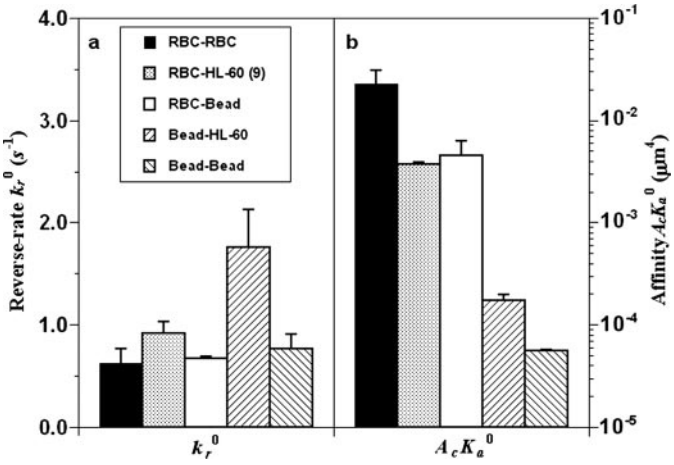

FIGURE 5. **Kinetic parameters obtained from best-fitting the binding curves to Equation 1.** Data are presented as mean ± S.D. of reverse rates, k_r^0 (*a*), and of effective binding affinities, $A_cK_a^0$ (*b*), for five configurations of RBC-RBC (*solid bars*), RBC-HL-60 (*dotted bars*) (9), Bead-RBC (*open bars*), Bead-HL-60 (*left-hatched bars*), and Bead-Bead (*right-hatched bars*).

curves were measured using the micropipette aspiration assay. As exemplified in Fig. 4, *a* and *b*, an ~8.7-fold higher site density was required for PSGL-1-coated beads than for PSGL-1-coated RBCs to reach the same level of steady-state adhesion frequency $P_a(\infty) \sim 0.4$ (comparing the *upper solid curve* at $m_l \times m_r = 19.9 \times 7.9 = 157.2$ μm^{-4} in Fig. 4*b* with the lower solid curve at $m_l \times m_r = 4.9 \times 3.7 = 18.1$ μm^{-4} in Fig. 4*a*). By comparison, the time required to reach the half-equilibrium binding level, $t_{1/2}$, was the same. Because the equilibrium binding $P_a(\infty)$ is related to the binding affinity, $A_cK_a^0 = -\ln[1 - P_a(\infty)]/(m_r \times m_l)$, and the half-time $t_{1/2}$ is related to the reverse rate, $k_r^0 \approx 0.5/t_{1/2}$ (24, 28), our data indicated that interacting PSGL-1 presented on the stiff carrier bound P-selectin with a lower effective binding affinity but a similar reverse rate compared with those presented on the soft carrier. These observations were confirmed by comparing the kinetic parameters obtained from fitting Equation 1 to the P_a *versus* t curves. The zero-force reverse rates for PSGL-1 coated on beads and RBCs were similar ($k_r^0 = 0.7 \pm 0.1$ and 0.6 ± 0.1 s^{-1}, respectively, $p > 0.65$). By contrast, the binding affinity for PSGL-1-coated beads was 4.9-fold lower than that for PSGL-1 coated on RBCs ($A_cK_a^0 = (4.55 \pm 1.77) \times 10^{-3}$ and $(2.25 \pm 0.79) \times 10^{-2}$ μm^4, respectively, $p < 0.09$) (*open* and *solid bars* in Fig. 5). The effective forward rate (calculated from $A_ck_f^0 = A_cK_a \times k_r^0$) for PSGL-1-coated beads was 4.6-fold lower than that for PSGL-1 coated on RBCs ($A_ck_f^0 = 3.06 \times 10^{-3}$ and 1.40×10^{-2} $\mu m^4/s$, respectively). This isolation of stiffness effects to the forward rate suggests that ligands presented on the soft carrier enhance accessibility for receptors on the apposing surface. It follows from this hypothesis that the dissociation of the preformed receptor-ligand bond would not be affected by stiffness, as was observed.

The above hypothesis was further tested by comparing the binding of P-selectin constructs coated on a soft RBC and a stiff bead to a PSGL-1-coated mAb bead, respectively, to form two configurations of RBC-Bead (Fig. 2, *c* and *c′*) and Bead-Bead (Fig. 2, *e* and *e′*). Here, a much higher site density of $m_l \times m_r = 24.9 \times 72.5 = 1805.3$ μm^{-4} was required for sPs-coated beads to reach the lower steady-state adhesion frequency $P_a(\infty) \sim 0.09$, whereas the much lower densities of $m_l \times m_r = 19.9 \times 3.5 = 68.7$ μm^{-4} was required for sPs-coated RBCs to reach the higher $P_a(\infty) \sim 0.33$ (comparing the *upper solid curve* in Fig. 4*d* with the *lower solid curve* in Fig. 4*b*). This translates to a 82-fold lower binding affinity for sPs-coated beads than RBCs ($A_cK_a^0 = (5.54 \pm 0.12) \times 10^{-5}$ and $(4.55 \pm 1.77) \times 10^{-3}$ μm^4, respectively, $p < 0.08$). By comparison, the zero-force reverse rates for sPs-coated beads and RBCs were similar ($k_r^0 = 0.8 \pm 0.1$ and 0.7 ± 0.1 s^{-1}, respectively, $p > 0.4$) (*right-hatched* and *open bars* in Fig. 5). The calculated effective forward rate for sPs-coated beads was 72-fold lower than that for RBCs ($A_ck_f^0 = 4.26 \times 10^{-5}$ and 3.06×10^{-3} $\mu m^4/s$, respectively). A similar test was also performed by comparing the two configurations of Bead-Bead (Fig. 2, *e* and *e′*) and RBC-RBC (Fig. 2, *a* and *a′*), which reads out a 405-fold lower binding affinity ($(5.54 \pm 0.12) \times 10^{-5}$ and $(2.25 \pm 0.79) \times 10^{-2}$ μm^4, respectively, $p < 0.06$) but the similar reverse rate ($k_r^0 = 0.8 \pm 0.1$ and 0.6 ± 0.1 s^{-1}, respectively, $p > 0.4$) for both sPs and PSGL-1 coated on beads than for both coated on RBCs (*right-hatched* and *solid bars* in Fig. 5). The calculated effective forward rate for Bead-Bead configuration was 328-fold lower than that for RBC-RBC configuration ($A_ck_f^0 = 4.26 \times 10^{-5}$ and 1.40×10^{-2} $\mu m^4/s$, respectively). These data support the validity of our hypothesis that carrier stiffness affects the forward rate but not the reverse rate of receptor-ligand interactions.

Enhancing Carrier Stiffness Reduces the Binding Affinity—Two more tests were done to confirm the above mechanism of stiffness effect. One test was to alter the carrier stiffness by varying the suction pressure on RBCs. Here sPs-coated RBCs were pressurized at a suction pressure of 4, 8, and 12 mm H_2O at a constant osmolarity of 175 mOsm and then bound to PSGL-

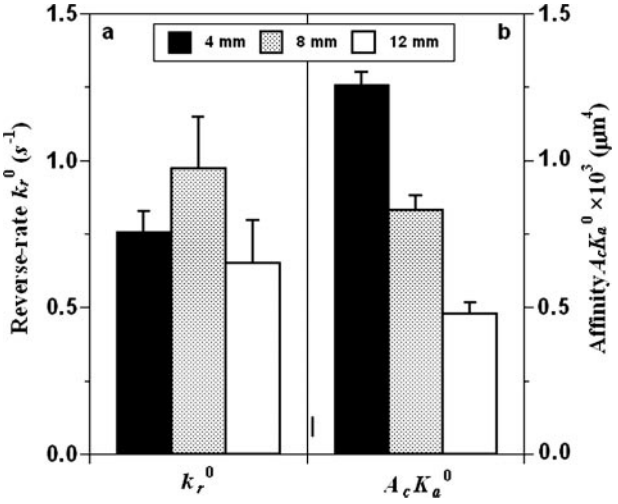

FIGURE 6. **Kinetic parameters at different suction pressures of 4 (*solid bars*), 8 (*dotted bars*), and 12 mm H_2O (*open bars*) (corresponding to 29.4, 59.8, and 88.2 pN/μm^2, respectively).** Data are presented as mean ± S.D. of reverse rates, k_r^0 (*a*), and effective binding affinities, $A_cK_a^0$ (*b*), for the RBC-HL-60 configuration.

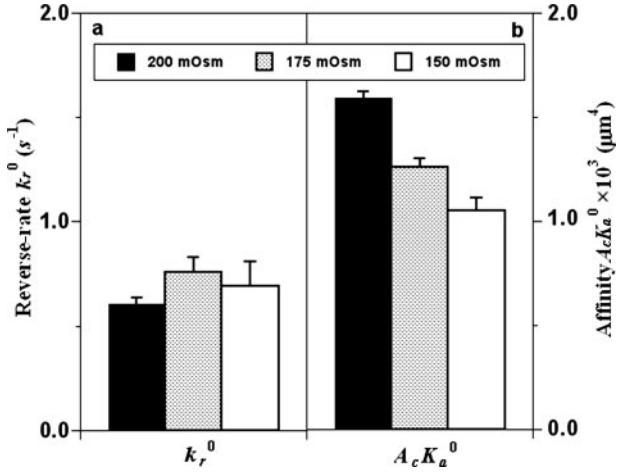

FIGURE 7. **Kinetics parameters at different osmotic resistances of 200 (*solid bars*), 175 (*dotted bars*), and 150 mOsm/kg (*open bars*) (corresponding to the ratios of H_2O:HBSS = 1:1, 1:1.4, and 1:2, respectively).** Data are presented as mean ± S.D. of reverse rates, k_r^0 (*a*), and effective binding affinities, $A_cK_a^0$ (*b*), for the RBC-HL-60 configuration.

1-expressed HL-60 cells. At the given site densities of $m_l \times m_r = 14.0 \times 50.2 = 702.8\ \mu m^{-4}$, sPs-coated RBCs bind to PSGL-1-expressed HL-60 cells at $P_a(\infty) = 0.59$, 0.44, and 0.28 at the respective suction pressure of 4, 8, and 12 mm H_2O (P_a *versus t* curves not shown). This translates to the moderate reduction in binding affinities ($A_cK_a^0 = (1.26 \pm 0.04)$, (0.83 ± 0.05), and $(0.48 \pm 0.04) \times 10^{-3}\ \mu m^4$, respectively) when suction pressure was enhanced from 4 through 12 mm H_2O (Fig. 6*b*). By comparison, the zero-force reverse rates at three suction pressures were similar ($k_r^0 = 0.8 \pm 0.1$, 0.9 ± 0.2 and $0.6 \pm 0.1\ s^{-1}$, respectively) (Fig. 6*a*).

Another test was to alter the carrier stiffness by swelling RBCs with different osmolarities of the medium. Here RBCs were swollen in three osmolarities of 200, 175, and 150 mOsm (corresponding to three concentrations of H_2O:HBSS: 1:2, 1:1.4, and 1:1, respectively), and adhesion measurements were performed at 4 mm H_2O. At the same site density as above, sPs-coated RBCs bound to PSGL-1-expressed HL-60 cells at $P_a(\infty) = 0.67$, 0.59, and 0.52 at the respective osmolarity of 200, 175, and 150 mOsm (P_a *versus t* curves not shown). This translates to the moderate reduction in binding affinities ($A_cK_a^0 = (1.59 \pm 0.05)$, (1.26 ± 0.04), and $(1.05 \pm 0.06) \times 10^{-3}\ \mu m^4$, respectively) when osmolarity was reduced from 200 through 150 mOsm (Fig. 7*b*). By comparison, the zero-force reverse rates at three suction pressures were similar ($k_r^0 = 0.6 \pm 0.0$, 0.8 ± 0.1 and $0.7 \pm 0.1\ s^{-1}$, respectively) (Fig. 7*a*). It was also indicated that the site density of the molecule of interest did not vary significantly when increasing suction pressure or decreasing medium osmolarity (data not shown). Taken together, even though the wider range alteration in suction pressure and medium osmolarity is unavailable in the micropipette aspiration assay, the moderate differences in binding affinity still provide additional support to the hypothesis that stiffening the molecular carrier reduced the receptor-ligand interactions.

Surface Microtopology Affects Two-dimensional Kinetics—To quantify the effects of surface microtopology on two-dimensional kinetics of receptor-ligand interactions, PSGL-1 coated on the RBC surface (Fig. 2, *a* and *a′*) and constitutively expressed on the HL-60 cell surface (Fig. 2, *b* and *b′*) bound to a P-selectin-coated RBC, respectively, to form two configurations of RBC-RBC and RBC-HL-60. Experiments for the latter configuration were done in a previous study (9). The binding affinity for PSGL-1 on HL-60 cells was 6.1-fold lower than PSGL-1 on RBCs ($A_cK_a^0 = (3.71 \pm 0.16) \times 10^{-3}$ and $(2.25 \pm 0.79) \times 10^{-2}\ \mu m^4$, respectively, $p < 0.08$). By comparison, the zero-force reverse rates were similar for both configurations ($k_r^0 = 0.9 \pm 0.1$ and $0.6 \pm 0.1\ s^{-1}$, respectively, $p > 0.15$) (*dotted* and *solid bars* in Fig. 5). The calculated effective forward rate for PSGL-1 on HL-60 cells was 4.1-fold lower than that for PSGL-1 on RBCs ($A_ck_f^0 = 3.40 \times 10^{-3}$ and $1.40 \times 10^{-2}\ \mu m^4/s$, respectively). PSGL-1 molecules were constitutively expressed on the stiffer and rougher surface of an HL-60 cell, compared with those coated onto an RBC. Stiffening the carrier and roughing the surface would have a cooperative effect on reducing the binding. It follows from this hypothesis that the dissociation of the preformed receptor-ligand bond would not be affected by microtopology, as was observed.

It is evident that the changes in surface roughness are invariably accompanied by a change in carrier stiffness, which induces the combined impact on two-dimensional kinetics of receptor-ligand interactions. To further test this, the binding of a PSGL-1-expressed HL-60 cell (Fig. 2, *b* and *b′*) or a PSGL-1-coated bead (Fig. 2, *c* and *c′*) to a P-selectin-coated RBC were compared in RBC-HL-60 and RBC-Bead configurations. The binding affinity, reverse rate, and calculated forward rate for PSGL-1 on HL-60 cells were similar to those for PSGL-1 on beads ($A_cK_a^0 = (3.71 \pm 0.16) \times 10^{-3}$ and $(4.55 \pm 1.77) \times 10^{-3}\ \mu m^4$, respectively, $p > 0.57$; $k_r^0 = 0.9 \pm 0.1$ and $0.7 \pm 0.0\ s^{-1}$, respectively, $p > 0.09$; $A_ck_f^0 = 3.40 \times 10^{-3}$ and $3.06 \times 10^{-3}\ \mu m^4/s$, respectively). PSGL-1 molecules were expressed on the relatively softer and rougher surface of an HL-60 cell, compared with those coated onto a bead. Softening the carrier and roughing the surface would have the opposing effects on binding, and the combined outcome indicated the similar two-dimensional binding kinetics in the two configurations.

Similar testing on the combined impact was done by comparing the binding of a PSGL-1-expressed HL-60 cell (Fig. 2, *d* and *d′*) or a PSGL-1-coated bead (Fig. 2, *e* and *e′*) to a P-selectin-coated bead in Bead-HL-60 and Bead-Bead configurations. The binding affinity for PSGL-1 on HL-60 cells was 3.1-fold higher than PSGL-1 on beads ($A_cK_a^0 = (1.72 \pm 0.26) \times 10^{-4}$ and $(5.54 \pm 0.12) \times 10^{-5}$ μm^4, respectively, $p < 0.03$). The zero-force reverse rate was 2.3-fold higher for PSGL-1 on HL-60 cells than on beads ($k_r^0 = 1.8 \pm 0.4$ and 0.8 ± 0.1 s^{-1}, respectively, $p = 0.071$) (*left-* and *right-hatched bars* in Fig. 5), which is still comparable to those reported in the literature (29–30). The calculated effective forward rate for PSGL-1 on HL-60 cells was 7.1-fold higher than PSGL-1 on beads ($A_ck_f^0 = 3.04 \times 10^{-4}$ and 0.43×10^{-4} $\mu m^4/s$, respectively). The observation that the binding was enhanced in the Bead-HL-60 configuration suggested that the changes in two-dimensional kinetics not only depend on the combined impact of stiffness and microtopology of a PSGL-1-bearing carrier, but also are associated with the relevant effects of an apposed P-selectin-bearing carrier.

Lack of Effects of Stiffness and Microtopology on the Three-dimensional Affinity—The isolation of the effects of carrier stiffness and microtopology to the forward rate (cf. Fig. 2, *a–c* and *e*) suggests that stiffening and roughing the carrier onto which a receptor is anchored reduce its accessibility by the binding partner anchored to the apposing surface. This hypothesis predicts that the effects of carrier stiffness and microtopology are associated primarily with two-dimensional binding, and will reduce or even diminish if the counter molecules are no longer restricted by their surface anchor. To further test this prediction, the solution affinities were compared between sPs-coated RBCs and beads and between PSGL-1-expressed HL-60 cells and PSGL-1-coated beads. Because sufficient soluble sPs and PSGL-1 were unavailable, the three-dimensional affinities were measured using ^{125}I-labeled G1 or PL1 mAb by Scatchard plot analysis (9, 17, 28). The three-dimensional affinity obtained from the negative slope of the linear fit to the Scatchard plot was similar for sPs-coated RBCs and beads (0.23 ± 0.02 and 0.20 ± 0.01 nM^{-1}, respectively; $p > 0.015$), and for PSGL-1-expressed HL-60 cells and PSGL-1-coated beads (0.31 ± 0.11 and 0.30 ± 0.08 nM^{-1}, respectively; $p > 0.5$) (Fig. 8*a*). These results support our prediction and suggest that stiffening the carrier and roughing the surface do not remarkably alter the conformation of the binding region of the molecule of interest.

To further confirm our prediction regarding the effects of carrier stiffness and microtopology on two-dimensional (but not on three-dimensional) affinity and kinetics, micropipette experiments were performed to measure at $t_0 = 4$ s the adhesion probability of the same mAb G1 (coated on RBC via $CrCl_3$ coupling) to the same sPs-coated RBC or bead, or of the same mAb PL1 (coated on RBC via $CrCl_3$ coupling) to the same HL-60 cell or PSGL-1-coated bead, used in the above three-dimensional affinity experiment. The results were expressed as $y = -\ln[1 - P_a(t_0)]/(m_r \times m_l) = A_cK_a^0[1 - \exp(-k_r^0 t_0)]$ according to Equation 1 (Fig. 8*b*). The differences in the measured $-\ln[1 - P_a(t_0)]/(m_r \times m_l)$ values most likely reflect different two-dimensional affinities, or more precisely, different forward rates (9). As expected, strong stiffness and microtopology effects were clearly observable (Fig. 8*b*; $p < 0.005$). The qualitatively similar effects of carrier stiffness and microtopology observed indicate the biophysical rather than biological basis of such effects, which do not depend on whether the molecules are constitutively expressed on the HL-60 cell surface or chemically coated on the RBC or bead surface via $CrCl_3$ coupling.

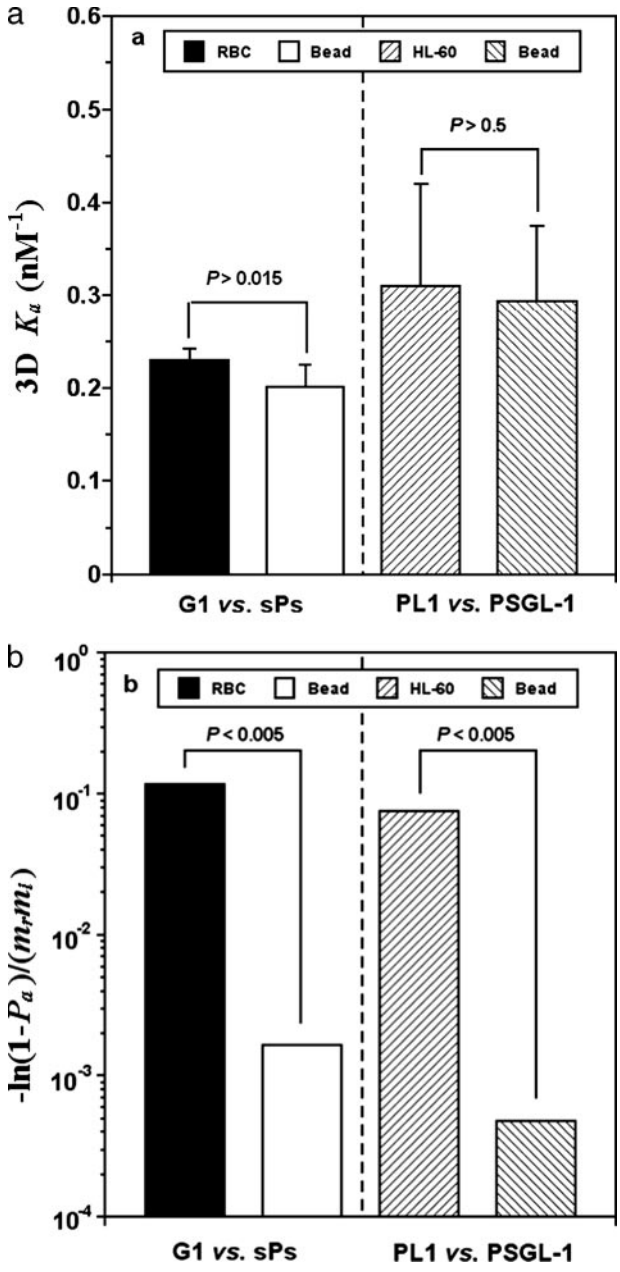

FIGURE 8. **Three-dimensional affinity and two-dimensional binding of G1 to P-selectin and of PL1 to PSGL-1 constructs.** *a*, Scatchard plot analysis for the three-dimensional affinity of binding of ^{125}I-labeled mAb G1 to sPs-coated RBCs (*solid bar*, data from Ref. 9) and beads (*open bar*), respectively, and of ^{125}I-labeled mAb PL1 to PSGL-1-expressed HL-60 cells (*left-hatched bar*) and PSGL-1-coated beads (*right-hatched bar*), respectively. Data are presented as means ± S.E. of the three-dimensional affinity. *b*, two-dimensional binding of G1-coated RBC to sPs-coated RBCs (*solid bar*) and beads (*open bar*), respectively, and of PL1-coated RBC to PSGL-1-expressed HL-60 (*left-hatched bar*) and PSGL-1-coated beads (*right-hatched bar*), respectively, measured at 4-s contact time. Data are presented as mean ± S.D. of $y = -\ln[1 - P_a(t_0)]/(m_r \times m_l)$. *p* value indicates the level of statistical significance of the differences in parameters for different carrier stiffness and microtopology.

DISCUSSION

The goal of the present study was to quantify the effects of different stiffness and microtopology of molecule-bearing carrier in terms of two-dimensional kinetics of receptor-ligand binding. In addition, kinetic and affinity measurements in both two-dimensional and three-dimensional binding were used to elucidate the biophysical basis of such effects. Three types of molecular carriers, including human RBC with deformable and relatively smooth surface, human HL-60 cell with less deformable and rough surface, and polystyrene bead with stiff and smooth surface, were used to achieve five configurations in adhesion frequency measurements (Fig. 2, *a*–*e* and *a*′–*e*′). The four types of configurations (Fig. 2, *a*–*c* and *e*) were found to reduce the two-dimensional forward rate but not the reverse rate (Figs. 4–7). In addition, neither type of configurations seemed to affect the three-dimensional binding affinity (Fig. 8*a*).

The two-dimensional adhesion assay requires the anchorage of receptors or ligands onto a carrier (cell or substratum) surface. Thus, surface presentation of a molecule affects the binding to its counterpart molecule. Two aspects of surface presentation are the orientation and length of molecule of interest above the carrier surface. For example, the binding of PSGL-1 was reduced remarkably by randomizing the orientation and/or shortening the length of P-selectin (9). Another two aspects are the stiffness and microtopology of the molecular carrier. The binding of hIgG to CD16b constructs coated onto RBCs were reduced ~50-fold lower when CD16b constructs were expressed onto CHO or K562 cells (10). Intact neutrophils with extensible microvilli facilitate the tether formation and rolling over P-selectin-immobilized substrate, whereas the fixed neutrophils or PSGL-1-coated beads do not (11). Even with the same orientation and length (cf. RBC-RBC, RBC-Bead, and Bead-Bead configurations in Fig. 2), the binding of P-selectin-PSGL-1 was significantly different (Fig. 5*b*). Alternatively, the dissociation among the above three configurations was the same (Fig. 5*a*).

Our data indicated that the carrier stiffness and microtopology affected the forward rate but not the reverse rate in four configurations (Fig. 2, *a*–*c* and *e*). Stiffening the carrier reduces the accessibility of a receptor to a ligand on apposing surface, because the ability for soft carrier to favor the accessibility is restricted when two carriers are driven to contact. Roughing the surface reduces the effective contact area A_c, which in turn reduces the effective binding affinity $A_cK_a^0$ or forward rate $A_ck_f^0$ because PSGL-1 molecules are evenly distributed onto the surface of the HL-60 cell (9, 25). This reasoning suggests that P-selectin or PSGL-1 presented onto the softer and smoother surface is more effective to bind PSGL-1 or P-selectin on the apposing surface, as was observed (Figs. 4–7). The dissociation of the preformed receptor-ligand bond, however, is not affected by the stiffness and microtopology, because the conformation of the molecular complex is not changed with different carrier stiffness and microtopology.

The isolation of such effects to the forward rate suggests a common biophysical mechanism. This mechanism predicts the combined impact of carrier stiffness and surface microtopology on two-dimensional kinetics when molecules are anchored on the carrier surface. Softening the carrier and smoothing the surface enhance the binding, whereas stiffening the carrier and roughing the surface reduce the adhesion. The combined outcome depends on which aspect plays the more important role in regulating the binding. Regardless of the experimental difficulties to further isolate both aspects, our results indicated that the combined impact reduced two-dimensional affinity for P-selectin or PSGL-1 anchored onto the stiff and rough surface.

These observed facts also suggest that different presentation methods of molecules on three types of carriers would affect the accessibility but not the stability. Capturing the molecules via non-blocking mAbs on RBCs results in an intermediate degree of uniformity in orientation as the capturing mAbs themselves were randomly coated on RBC via $CrCl_3$ coupling. Coating the molecules via biotin-streptavidin coupling on beads provides similar uniformity as the biotinylated capturing mAbs bind randomly to streptavidin-coated beads. PSGL-1 ligands are constitutively expressed on the microvilli tips of HL-60 cells with the uniform orientation. Our data indicated that soluble G1 or PL1 mAb binds similarly to P-selectin or PSGL-1 presented in the above different ways (Fig. 8*a*), suggesting that the effect of carrier stiffness and microtopology reported here would not be influenced by the presenting methods used.

The lateral diffusion of interacting molecules on RBC membrane might play a role in affecting the two-dimensional binding. This should be true when the molecules are constitutively expressed on such a dynamic biological membrane and are free to diffuse laterally into the contact zone. However, this is not the case for RBC in the current work. Here P-selectin or PSGL-1 molecules coupled onto the RBC surface were hard to diffuse freely because they were captured on the surface by capturing mAbs (S12 or PL2), which were covalently linked by the -COOH group on RBC membrane via $CrCl_3$ (20). Such coupling reduces remarkably the lateral diffusion of molecules of interest and the recruitment of molecules into the contact zone, which is comparable to the case for streptavidin beads where biotinylated capturing mAbs (S12 or PL2) were linked by biotin-streptavidin interactions on the bead surface. Another line of reasoning is that the RBC held on a micropipette by suction pressure has surface tension, and the molecules captured on the RBC surface are more difficult to diffuse. In this sense, it is reasonable to neglect the effect of lateral diffusion when the molecules are covalently coupled onto the surface of RBC, which is beyond the scope of the current work.

Finally, the present work provides not only quantitative measurements of the effects of two aspects of molecule presentation of adhesion, carrier stiffness, and microtopology, on their two-dimensional binding affinity and kinetics, but also insights into the biophysical basis of such effects.

Acknowledgments—We thank Dr. R. P. McEver for the generous gifts of sPs, S12, G1, PL1, and PL2 proteins, Dr. Periasamy Selvaraj for the generous gift of TS2/9 protein, Drs. J. G. Geng, L. Li, and Z. Z. Ye for PSGL-1 purification. We also thank Dr. C. Zhu for helpful discussions.

REFERENCES

1. Hynes, R. O. (2002) *Cell* **110,** 673–687
2. McEver, R. P. (2001) *Thromb. Haemost.* **86,** 746–756

3. Vestweber, D., and Blanks, J. E. (1999) *Physiol. Rev.* **79,** 181–213
4. McEver, R. P. (2002) *Curr. Opin. Cell Biol.* **14,** 581–586
5. Moore, K. L., Patel, K. D., Bruehl, R. E., Li, F., Johnson, D. A., Lichenstein, H. S., Cummings, R. D., Bainton, D. F., and McEver, R. P. (1995) *J. Cell Biol.* **128,** 661–671
6. Li, S. H., Burns, D. K., Rumberger, J. M., Presky, D. H., Wilkinson, V. L., Anostario, Jr., M., Wolitzky, B. A., Norton, C. R., Familletti, P. C., Kim, K. J., Goldstein, A. L., Cox, D. C., and Huang, K. S. (1994) *J. Biol. Chem.* **269,** 4431–4437
7. Leppänen, A., Mehta, P., Ouyang, Y. B., Ju, T. Z., Helin, J., Moore, K. L., Die, I. V., Canfield, W. M., McEver, R. P., and Cummings, R. D. (1999) *J. Biol. Chem.* **274,** 24838–24848
8. Epperson, T. K., Patel, K. D., McEver, R. P., and Cummings, R. D. (2000) *J. Biol. Chem.* **275,** 7839–7853
9. Huang, J., Chen, J., Chesla, S. E., Yago, T., Mehta, P., McEver, R. P., Zhu, C., and Long, M. (2004) *J. Biol. Chem.* **279,** 44915–44923
10. Williams, T. E., Nagarajan, S., Selvaraj, P., and Zhu, C. (2001) *J. Biol. Chem.* **276,** 13283–13288
11. Park, E. Y. H., Smith, M. J., Stropp, E. S., Snapp, K. R., DiVietro, J. A., Walker, W. F., Schmidtke, D. W., Diamond, S. L., and Lawrence, M. B. (2002) *Biophys. J.* **82,** 1835–1847
12. Finger, E. B., Bruehl, R. E., Bainton, D. F., and Springer, T. A. (1996) *J. Immunol.* **157,** 5085–5096
13. Shao, J. Y., Ting-Beall, H. P., and Hochmuth, B. (1998) *Proc. Natl. Acad. Sci. U. S. A.* **95,** 6797–6802
14. Williams, T. E., Selvaraj, P., and Zhu, C. (2000) *Biophys. J.* **79,** 1858–1866
15. Dumaswala, U. J., Wilson, M. J., Jose, T., and Daleke, D. L. (1996) *Blood* **88,** 697–704
16. Ushiyama, S., Laue, T. M., Moore, K. L., Erickon, H. P., and McEver, R. P. (1993) *J. Biol. Chem.* **268,** 15229–15237
17. Geng, J. G., Bevilacqua, M. P., Moore, K. L., McIntyre, T. M., Prescott, S. M., Kim, J. M., Bliss, G. A., Zimmerman, G. A., and McEver, R. P. (1990) *Nature (Lond.)* **343,** 757–760
18. Moore, K. L., Eatonll, S. F., Lyons, D. E., Lichenstein, H. S., Cummings, R. D., and McEver, R. P. (1994) *J. Biol. Chem.* **269,** 23318–23327
19. Nagarajan, S., Chesla, S. E., Cobern, L., Anderson, P., Zhu, C., and Selvaraj, P. (1995) *J. Biol. Chem.* **270,** 1–9
20. Kofler, R., and Wick, G. (1977) *J. Immunol. Methods* **16,** 201–209
21. Selvaraj, P., Plunkett, M. L., Dustin, M., Sanders, M. E., Shaw, S., and Springer, T. A. (1987) *Nature* **326,** 400–403
22. Gretch, D. R., Suter, M., and Stinski, M. F. (1987) *Anal. Biochem.* **163,** 270–277
23. Long, M., Chen, J., Jiang, N., Selvaraj, P., McEver, R. P., and Zhu, C. (2006) *Biophys. J.* **91,** 352–363
24. Chesla, S. E., Selvaraj, P., and Zhu, C. (1998) *Biophys. J.* **75,** 1553–1572
25. Long, M., Zhao, H., Huang, K. S., and Zhu, C. (2001) *Ann. Biomed. Engi.* **29,** 935–946
26. Long, M., Goldsmith, H. L., Tees, D. F. J., and Zhu, C. (1999) *Biophys. J.* **76,** 1112–1128
27. Zhu, C., Long, M., Chesla, S. E., and Bongrand, P. (2002) *Ann. Biomed. Eng.* **30,** 305–314
28. Chesla, S. E., Li, P., Nagarajan, S., Selvaraj, P., and Zhu, C. (2000) *J. Biol. Chem.* **275,** 10235–10246
29. Merkel, R. (2001) *Phys. Rep.* **346,** 343–385
30. Hanley, W., McCarty, O., Jadhav, S., Tseng, Y., Wirtz, D., and Konstantopoulos, K. (2003) *J. Biol. Chem.* **278,** 10556–10561